IOP Publishing Smart Materials and Structures
Smart Mater. Struct. 26 (2017) 065017 (10pp) https://doi.org/10.1088/1361-665X/aa6ef0

Squeeze flow behavior of shear thickening fluid under constant volume

Xinglong Gong[1,3], Qian Chen[1], Mei Liu[2], Saisai Cao[1], Shouhu Xuan[1,3] and Wanquan Jiang[2]

[1] CAS Key Laboratory of Mechanical Behavior and Design of Materials, Department of Modern Mechanics, University of Science and Technology of China (USTC), Hefei 230027, People's Republic of China
[2] Department of Chemistry, USTC, Hefei 230026, People's Republic of China

E-mail: gongxl@ustc.edu.cn and xuansh@ustc.edu.cn

Received 21 March 2017, revised 16 April 2017
Accepted for publication 24 April 2017
Published 16 May 2017

Abstract

Squeeze flow behavior of shear thickening fluid (STF) consisting of SiO_2 particles and ethylene glycol (EG) was investigated. STF was squeezed out radially between the parallel plate accessory of rheometer. Due to formation of particle chains and alignment of clusters, an obvious increase in normal stress was found in the squeeze procedure. When the sample (71 wt% SiO_2) thickness was squeezed from 1 mm to 0.2 mm, normal stress rapidly increased from 0 Pa to 38.48 kPa. In comparison to the peak stress under shear mode (6.38 kPa), the squeeze stress of STF was larger. Moreover, it was found that normal stress was significantly enhanced at large squeeze velocity, large mass fraction and appropriate wall roughness. Meanwhile, shear viscosity under moving boundary was studied by applying a constant shear on STF during the squeeze test. Together with the shear effects, squeeze could change the inner particle distributions and affected the rheological property of STF. The related results were helpful for further understanding the shear thickening mechanism and developing new STF-based applications.

Keywords: shear thickening fluid, squeeze, normal stress, wall roughness, shear viscosity

(Some figures may appear in colour only in the online journal)

1. Introduction

Shear thickening is a kind of non-Newtonian flow behavior widely existing in dense particle suspensions [1–6]. Beyond a critical shear rate, the viscosity of shear thickening fluid (STF) may increase by orders of magnitude [7, 8]. Because of the unique shear thickening behavior, STF has attracted considerable interests in soft armor, dampers, impact absorbers and control devices [9, 10]. Manufacture of these applications and their subsequent functional materials usually involves flow geometries substantially from that of simple shear flow experiments [11]. Vibration control devices can be classified into three working modes: direct shear mode, valve mode and squeeze flow mode [12–14]. Most of the STF-based dampers are designed under direct shear mode or valve mode. It is found that damping force under squeeze flow mode is larger than that under the other two modes [14, 15]. Thus, it is important to investigate the squeeze flow behavior of STF, which will contribute to developing high-performance STF devices under squeeze flow mode.

As a typical non-Newton fluid, the squeeze flow behavior of STF can be carried out by placing the measured sample between two parallel plates and then squeeze out the sample radially. This form of squeeze is often used for small amplitude vibration dampers [16]. Considering the geometry between STF and plates, two different squeeze modes can be selected: constant area mode and constant volume mode [16–19]. In the constant area mode, the sample radius gradually grows larger than the plate. Sample will be squeezed out of the plate during the test. In the constant volume mode, the sample radius is smaller than the plate and the radial interface is free [16, 17]. Using a constant area parallel plate apparatus, sealing effect is responsible for squeezing out an unknown quantity of particles from the sample between the

[3] Authors to whom any correspondence should be addressed.

plates, resulting in the change of particle concentration between the parallel plates [18]. To avoid these restrictions, constant volume mode is adopted here in investigating the squeeze flow behavior of STF.

Squeeze flow rheometer has been used for investigating the squeeze flow between two plates. The velocity profile between the plates cannot be exactly obtained, but only the total force is measured. Measured normal stress is an average value over the surface of the plate [19]. The lubrication limit in the inner region of the gap and the pressure in the adjacent outer region of the gap play an important role in the squeeze flow of a power-law fluid between rigid spheres. Thus, the approximate Herschel–Bulkley relationship may be written in the following form: $\tau = \tau_0(1 + \varphi\dot{\gamma}^m)$, where τ_0 is the shear yield stress, m the shear plastic flow index, $\varphi = k/\tau_0$ and k is shear plastic consistency [20]. Wall slip would result in a reduction in the viscous force and has a profound effect on shear thickening material [21]. Moreover, the geometrical characteristics of plates significantly influence the squeeze flow. Surface microchannels can accelerate squeezing flow of a fluid in a thin gap between parallel plates [22]. If the plates are non-parallel, the plate inclination can apparently affect the force produced by the squeeze flow [23].

Squeeze and tensile are both typical normal deformations. Much effort has been done to study the tensile behavior of STF but the squeeze behavior is seldom investigated [11, 24, 25]. The tensile properties of STF are studied by a filament-stretching rheometer [11]. At a critical strain rate, a dramatic increase in both speed and magnitude of the strain-hardening is observed in STF. With the continuous increasing of the strain rate, STF undergoes a transition from liquid-like breakup to a fracture mode, which can be linked to the dilatancy and jamming of the suspensions [11]. At the same time, strong viscoelasticity can be observed during the transition. The strain-hardening is attributed to the formation of strings and alignment of clusters in the flow direction, similar to the shear thickening mechanism [24]. Similar to the tensile behavior, squeeze behavior should also be an important aspect to comprehend the structure evolution of STF. At the same time, shear viscosity is closely associated with the inner structure evolution [26–29]. Critical shear rate of STF strongly increases with the increasing gap in a simple shear flow [30]. To this end, studying the shear viscosity of STF in the squeeze mode will contribute to understanding the rheological property under moving boundary. Moreover, the squeeze flow behavior of STF is important for understanding the shear thickening mechanism and developing effective STF-based applications. Therefore, it is necessary to investigate the squeeze flow behavior of STF comprehensively.

In this work, STFs of different mass fractions (61 wt%, 63 wt%, 65 wt%, 67 wt%, 69 wt% and 71 wt%) were prepared to experimentally study the squeeze flow behavior under constant volume. Plastic sandpapers with different mesh numbers were used to modify the surface. The influences of mass fraction, squeeze velocity and wall roughness on squeeze flow behavior were investigated, respectively. Moreover, shear viscosity of STF under different squeeze conditions was compared. Moving boundary conditions showed significant effects on the rheological property of STF.

2. Experimental section

2.1. Materials

The STFs were prepared by dispersing SiO_2 particles into ethylene glycol (EG). A small amount (0.5 wt%) of sodium dodecyl sulfonate (SDS), a kind of anionic surfactants, was also added to the suspensions to strengthen the shear thickening effect [31]. SiO_2 particles were obtained from industrial grinding. EG and SDS were purchased from Sinopharm Chemical Rea Co. Pretreatment was conducted on SiO_2 particles in order to remove the impurities. SiO_2 particles were dispersed in a solvent consist of ethyl alcohol and acetone (1/1, v/v) to be cleaned for 2 h by an ultrasonic cleaner [32]. The cleaned particles were dried in a vacuum oven (about 24 h) at 40 °C. Without the pre-processed procedure, there would be impurities in the STF sample and then the shear thickening effect was weakened. SiO_2 particles, EG and SDS were mixed in a ball grinding mill (QM-3SP2, purchased from Nanjing NanDa Instrument Plant, 230 r min^{-1}) for 24 h to obtain uniform suspensions. STFs with different SiO_2 particle mass fractions (61 wt%, 63 wt%, 65 wt%, 67 wt%, 69 wt% and 71 wt%) were prepared.

2.2. Apparatus

The squeeze flow behavior of STF was investigated primarily by a stress and strain controlled rheometer (Anton-Paar MCR 302) with the test accessory of PP43 (figure 1). PP43 was parallel plate accessory with a diameter of 43 mm. The STF sample was placed in the center of the plates during the test. The initial gap between parallel plates was set as 1 mm. A pre-shear procedure of 30 s was given at the beginning to allow the system to reach steady state. The shear rate at the pre-shear procedure was 1 s^{-1}. For squeeze measurements, the top plate pushed down at a constant velocity to squeeze the STF while the bottom plate was fixed. The experimental processes were carried out as follows. (1) 0.3 ml STF sample was placed between the parallel plates with a syringe. (2) A 30 s pre-shear procedure was conducted on the STF sample to make SiO_2 particles be uniformly distributed. (3) The squeeze measurements were started at a constant squeeze velocity. (4) When the gap between parallel plates reduced to 0.2 mm, the top plate turned to raise to the initial state at the same velocity. With the rheometer (MCR 302), shear rate could be applied on STF in the squeeze-tensile test. Therefore, shear viscosity during the squeeze-tensile procedure was investigated. When investigating the effect of squeeze on shear viscosity, a constant shear rate was also conducted on STF in step (3) and (4).

To investigate the effect of wall roughness on the normal stress, plastic sandpapers (figure 1(c)) with different mesh numbers were pasted on the surface of the parallel plate (figure 1(d)). The sandpaper and testing geometry PP-43 were

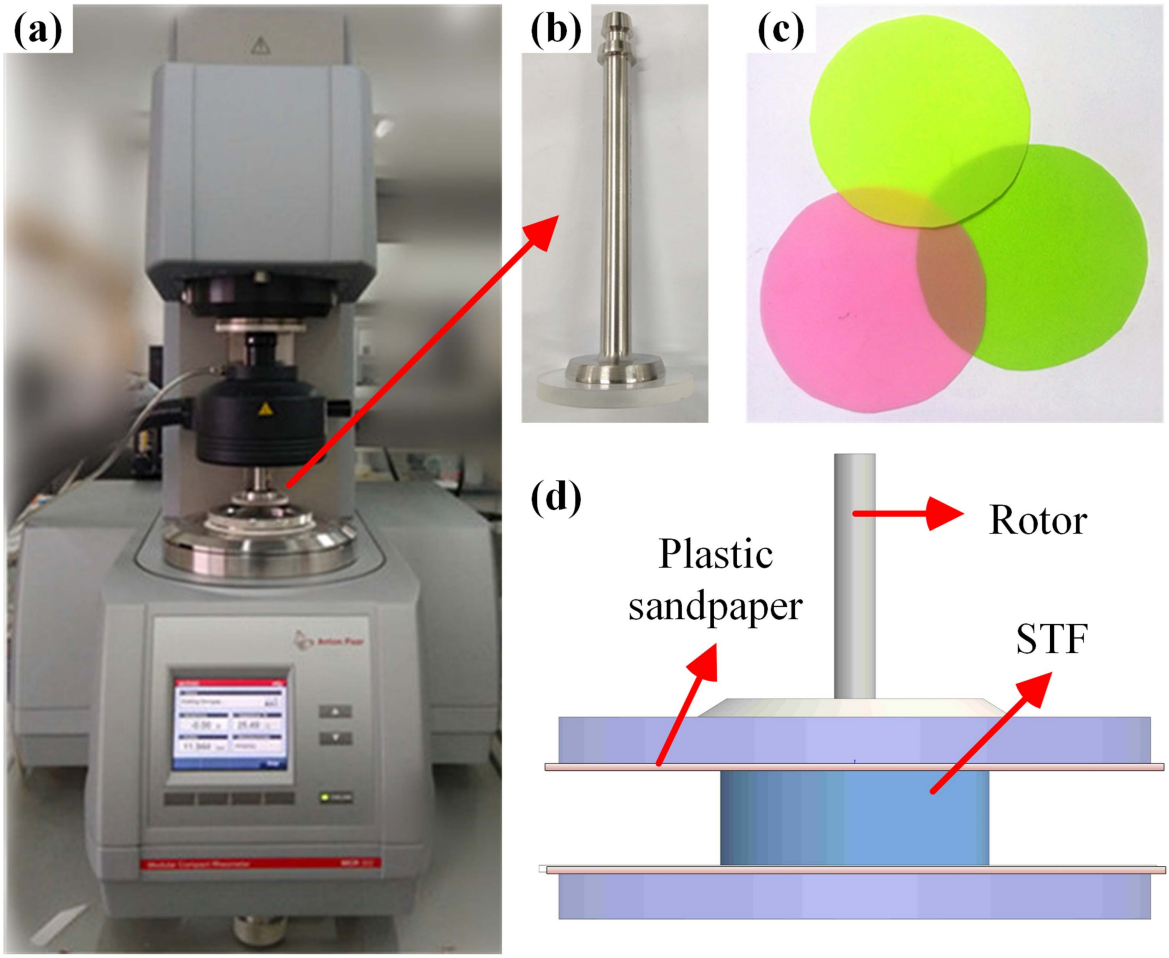

Figure 1. Schematic of the experiment device (a) stress and strain controlled rheometer (Anton-Paar MCR 302); (b) parallel plate accessory (PP-43); (c) plastic sandpaper; (d) modified parallel plate.

coaxial. The plastic sandpapers were purchased from 3M Company. Plastic sandpapers were manufactured by plating SiC sands on a plastic sheet. The diameter of SiC sands was used to distinguish the specifications of sandpapers. Surface of the PP-43 accessory was quartz crystal. In this work, 5 kinds of plastic sandpapers were used. The mesh numbers were 800, 2000, 6000, 10 000 and 12 500, which were named as S-1, S-2, S-3, S-4 and S-5, respectively. Quartz crystal surface was named as S-0. The relationship between mesh numbers and sand diameters were shown in table 1. Plastic sandpapers were cut into discs with a diameter of 44 mm, slightly larger than the diameter of the parallel plate. All the measurements were conducted at the temperature of 20 °C.

Table 1. Relationship between mesh numbers and sand diameters.

Mesh number	800	2000	6000	10 000	12 500
Sand diameter (μm)	18	6.5	2.1	1.3	1
Surface number	S-1	S-2	S-3	S-4	S-5

3. Results and discussions

3.1. Rheological property of STF

Figures 2(a) and (b) showed the SEM and TEM images of SiO_2. The microscope photographs indicated that the SiO_2 particles obtained from industrial grinding possessed irregular shape. The average particle diameter was around 2 μm. It could be found that the pre-treated SiO_2 particles were uniformly distributed and no terrible aggregation was found. Steady shear tests were conducted by the rheometer with a cone-plate accessory (CP25-2). Figure 2(c) showed the rheological property of all samples. With increasing of the SiO_2 mass fractions, interparticle contacts became obvious and the shear thickening effects were significantly strengthened. At low mass fraction, the viscosity gently increased in the shear thickening state. When the mass fraction increased from 61 wt% to 71 wt%, the peak viscosity drastically grew from 0.65 to 56.36 Pa s. STF sample showed apparent discontinuous shear thickening phenomenon when the mass fraction was 71 wt%.

3.2. Effect of squeeze velocity on squeeze flow behavior

Under squeeze, SiO_2 particles in STF spread out radially between the parallel plates. The interactions between particles varied quickly when particles get close to each other. Squeeze

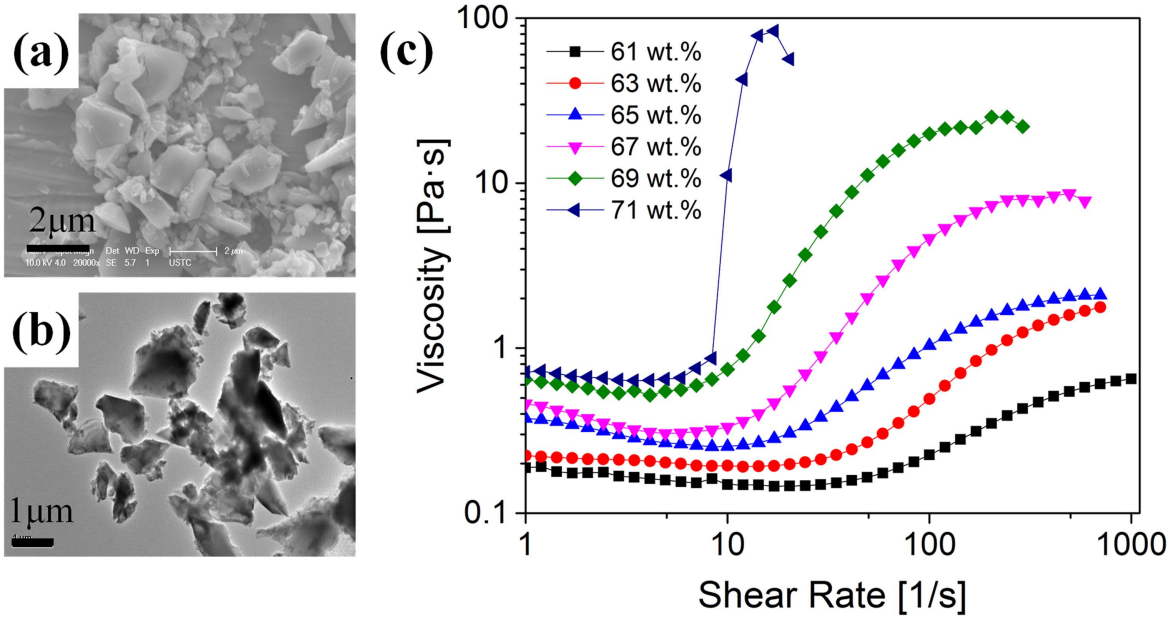

Figure 2. SEM (a) and TEM (b) of SiO_2 particles; (c) steady shear tests results of all samples.

velocity showed obvious effect on the normal stress of STF. Figure 3(a) was a typical squeeze curve of STF. Here, the mass fraction of the SiO_2 particles in STF was 71 wt% and the squeeze velocity was 300 μm s^{-1}. Compared with normal force, normal stress was more appropriate for describing the squeeze flow behavior of STF under constant volume. Normal stress could be obtained by the following equation:

$$\sigma = \frac{F_N}{S} = \frac{F_N}{V/h},$$

where σ was normal stress, F_N was measured normal force, S was the contact area between the sample and plate, h was the gap of parallel plates, V was the volume of STF. In this work, V was 0.3 ml. The curves of normal stress under squeeze could be divided to three stages: (1) Free spread of STF. Normal stress is almost zero in this state. (2) Viscous flow. After gap reduced below a critical value (critical gap), normal stress began to rise slowly. (3) Plastic flow. With the further reduction of the gap, a rapid increment in normal stress was found. When the gap reduced to 0.2 mm, the normal force reach a peak value.

Initial gap showed few effect on the squeeze flow behavior of STF. STF was a rate-dependent material, which meant that squeeze flow behavior was also dominated by the change of rate. Squeeze rate was defined as the ratio of squeeze velocity to plate gap. In the first stage, squeeze rate was relatively slow. SiO_2 particles in STF could easily spread together with the dispersing medium to the surroundings. In the second stage, there were was almost no contact between particles but squeeze rate became large. At this time, a rapid increase in the local shear rate existed in STF [21]. This increasing shear rate led to the uneven particle distributions and the liquid viscous force. The normal force was a reflection of the liquid viscous force between the particles. In the third stage, particles gradually contacted with each other and formed network structure. Thus, the spread of particles was impeded. When the network structure touched the boundary, jamming appeared in the suspensions, resulted in the increment of normal force. Generally, boundary in this work meant physical boundary. Interparticle contact force and friction determined the variation of normal force (figure 4).

When the squeeze velocity grew, squeeze flow behavior of STF showed obvious changes (figure 3(b)). Mass fraction of the sample was 71 wt% and the squeeze velocity was changed from 50 to 500 μm s^{-1}. At large squeeze velocity, the rapid change of squeeze rate caused the variation of particle distributions. Interactions between SiO_2 particles and dispersing medium were enhanced immediately. The formation of particle chains was brought forward. So the critical gap and the normal stress corresponding to the same gap both showed increasing tendency with the increasing of the squeeze velocity. For the reason that the rheometer could provide a maximum normal force of 50 N, the squeeze procedure would be stopped when the normal force reached the maximum value. Thus, sample of large particle concentrations could not be squeezed to 0.2 mm when the normal stress was relatively large.

The cycle-ability of the squeeze flow behavior was also investigated. Figures 3(c)–(d) depicted the variation of the normal stress during the squeeze/tensile cycles. The squeeze velocity of each cycle was all kept at 300 μm s^{-1}. It could be seen that the normal stress curves were almost coincident in 5 cycles. In the squeeze procedure, normal stress quickly rose to 25 kPa. When the sample was squeezed to 0.2 mm, the top plate turned back to the initial state at the same velocity. The peak normal stress in the tensile procedure was about 27 kPa. The surface of PP-43 was made of quartz crystal, a kind of glaze surface, so the normal stress curve in one squeeze/tensile cycle was nearly symmetric. This tensile procedure

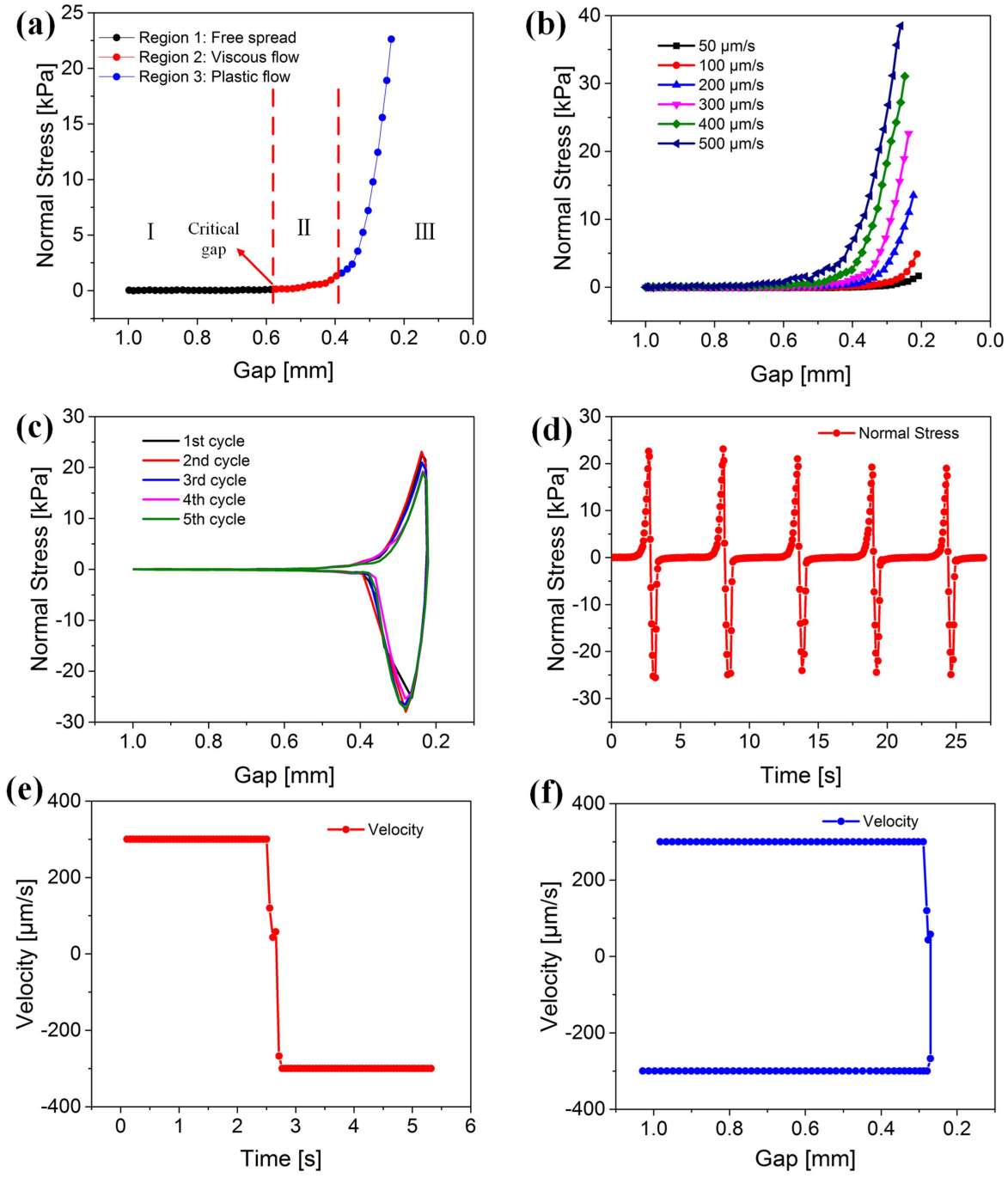

Figure 3. (a) A typical squeeze curve of STF; (b) change in normal stress with gap distance for different squeeze velocities; (c)–(d) changes in normal stress under squeeze/tensile cycles. Mass fraction of the sample was 71 wt%. The data curve of velocity versus time (e) and velocity versus gap (f).

could be regarded as an unloading process of squeeze. As the gap became large, the squeeze rate reduced. The strings and alignment of clusters gradually disappeared. The good repeatability enabled the STF to be applied under squeeze mode. Figures 3(e)–(f) were the data curve of velocity versus time and velocity versus gap, respectively. At the end of the squeeze procedure and the beginning of the tensile procedure, the velocity was smaller than 300 μm s^{-1} due to the instruments. This could also be regarded as the reason for the decrement of the normal force during the process of the squeeze-tensile conversion.

3.3. Effect of SiO_2 mass fraction on squeeze flow behavior

During the squeeze experiment, the top plate approached to the bottom plate, thus the contacts between SiO_2 particles became much easier with the increasing mass fractions. Mass fractions had a significant effect on the squeeze flow behavior of STF. Figure 5 showed the squeeze flow behavior of STF. The SiO_2 mass fractions varied from 61 wt% to 71 wt% while the squeeze velocity was fixed at 300 μm s^{-1}. Under squeeze, EG had little effect on the normal stress. The maximum normal stress, which corresponded to the minimum gap in the

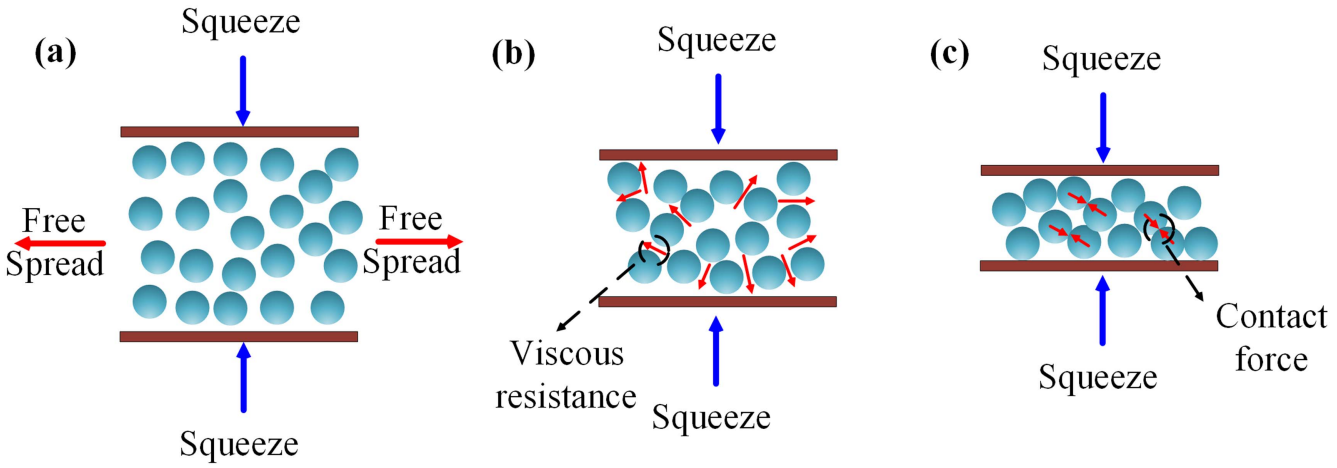

Figure 4. Schematic illustrations of the structure evolution under squeeze: (a) free spread; (b) viscous flow; (c) plastic flow.

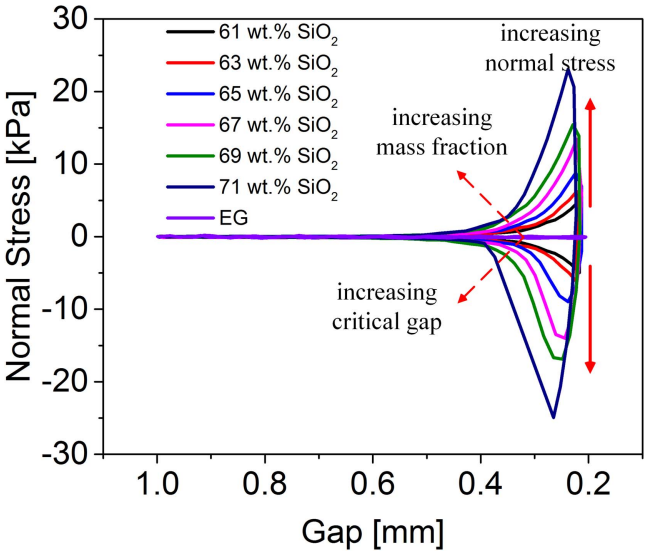

Figure 5. Change in the normal stress with gap distance for different SiO_2 mass fractions. Squeeze velocity was 300 μm s^{-1}.

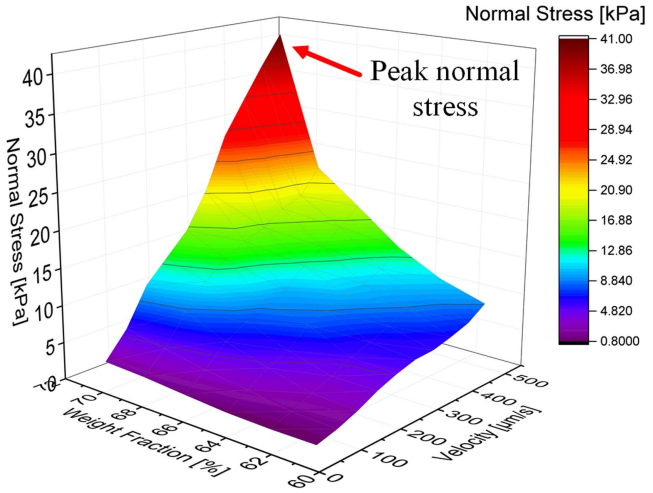

Figure 6. Combined effect of squeeze velocity and SiO_2 mass fraction on the normal stress.

squeeze procedure, increased from 4.95 kPa to 23.09 kPa with the increasing mass fractions. Meanwhile, critical gap apparently increased from 0.48 mm to 0.55 mm. Critical squeeze rate decreased from 0.625 s^{-1} to 0.545 s^{-1}. The critical gap was closely associated with the critical squeeze rate. The larger the mass fractions was, the larger the critical gap would be. So the critical squeeze rate generally decreased with the increasing mass fractions. Under constant volume, the interparticle distance decreased with the increasing mass fraction. It is much easier for particles to get contacts with each other. So SiO_2 particles formed chains and STF would become solid-like at short squeeze distance. Then critical gap increased with the increasing mass fraction. It could be concluded that the particle interactions were enhanced at large mass fractions, which would further induce a larger normal stress.

Figure 6 showed the combined effect of squeeze velocity and SiO_2 mass fraction on the squeeze flow behavior of STF. When the squeezed velocity changed, the peak normal stress still kept increasing with the increasing SiO_2 mass fraction. In general, high mass fraction and large squeeze velocity would promote the interactions between particles. Then, normal stress of STF under squeeze conditions was significantly enhanced under these circumstances. The peak normal stress could reach 38.48 kPa under squeeze. Compared with peak shear stress (6.38 kPa), STF could provide larger stress under squeeze mode. Thus, developing new STF devices under squeeze flow mode could significantly improve the working efficiency.

3.4. Effect of wall roughness on squeeze flow behavior

Under squeeze, the micron-sized SiO_2 particles interacted with the surface of the parallel plate accessory. Wall roughness would change the interactions between STF and the boundary, then affect the squeeze flow behavior. In order to investigate the effect of wall roughness on squeeze flow behavior, the parallel plate accessory was modified by pasting plastic sandpapers of different mesh numbers on the surface. The variation of normal stress during one squeeze-tensile cycle under modified parallel plate (figure 1(d)) was shown in figure 7(a). Different from the result when using the

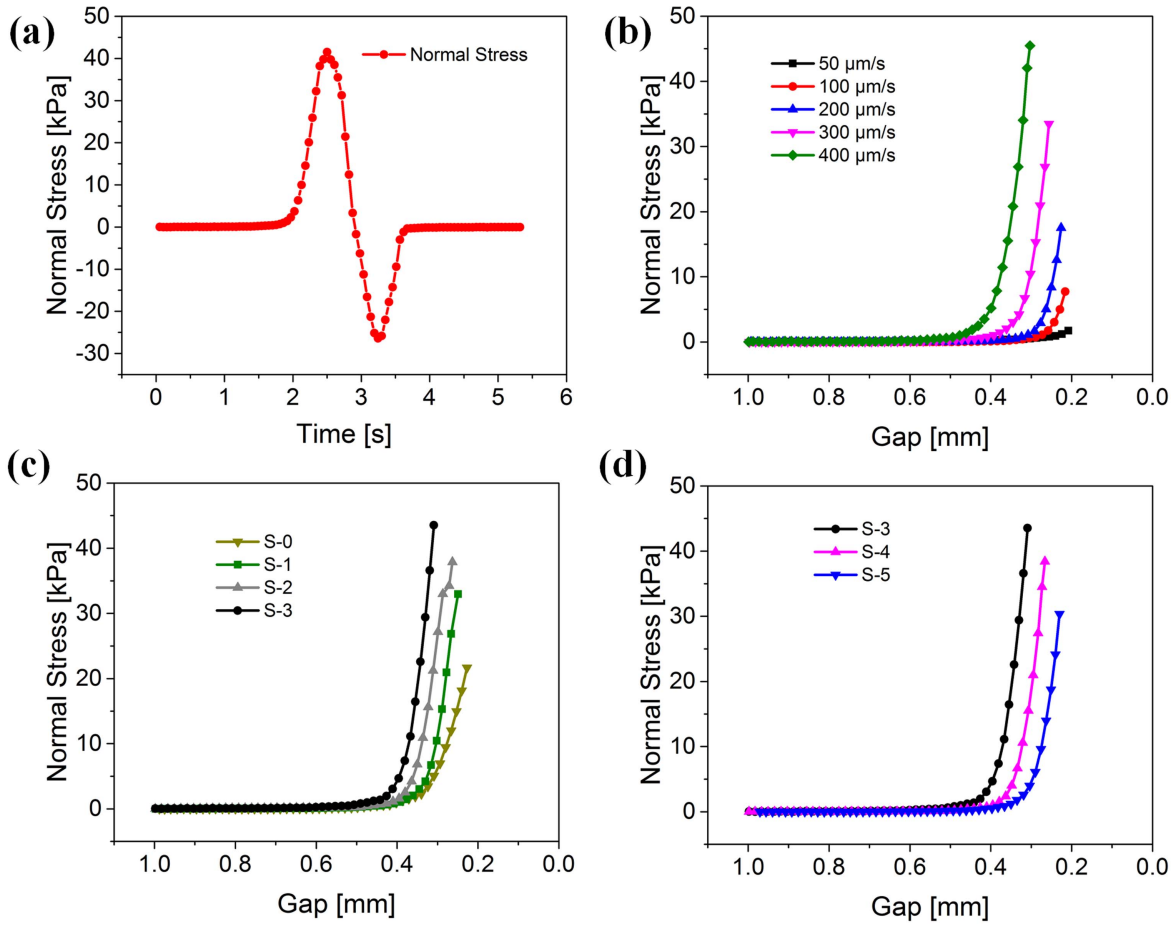

Figure 7. (a) The variation of normal stress under modified parallel plate during one squeeze-tensile cycle; (b) change in normal stress with gap distance for different squeeze velocities under modified parallel plate; (c) and (d) change in normal stress with gap distance for different surfaces. Mass fraction of the sample was 71 wt% and squeeze velocity was 300 μm s^{-1}.

unmodified parallel plate, this normal stress curve showed asymmetry. The peak normal stress (41.5 kPa) in the squeeze process was larger than that (26.4 kPa) in the tensile process. This result could be attributed to the effect of wall roughness. In granular suspensions of high concentration, the slip of chain structure mainly happened in the vicinity of the plate [33]. In the squeeze process, the rough surface of the pasted plastic sandpaper limited the movement of the particles, resulting in the increment of the normal stress. Meanwhile, the restriction of wall roughness on the particle movement in the squeeze mode was more obvious than that in the tensile mode. Thus, peak stress in the squeeze process was higher than that in the tensile process, especially at large squeeze velocity. Figure 7(b) showed the effect of squeeze velocity under modified parallel plate. Similar to the results in section 3.2, normal stress also increased with increasing of the squeeze velocity. Compared with the quartz crystal surface, the increment of normal stress in this case became larger due to the restriction of rough surface on the particle movement.

Wall roughness varied with the mesh numbers of plastic sandpapers. So squeeze flow behavior of STF was closely related to wall roughness (figures 7(c) and (d)). The squeeze velocity was 300 μm s^{-1}. It is noticed that the normal stress did not change monotonically with the mesh numbers of plastic sandpapers. The increment of normal stress was greatly enhanced when the mesh number was 6000. Mesh number of plastic paper was decided by the diameter of the plated sand. When mesh number was 6000, the sand diameter and the sand space were both 2.5 μm, nearly the same as the diameter of the SiO_2 particles. In this case, SiO_2 particles near the wall were subjected to restrictions of the sand. Friction between the wall and SiO_2 particles was greatly enhanced. The size matching of particles and sand space made particle movements difficult, resulting in the increasing of normal stress. When the mesh number was smaller than 6000, the sand diameter and sand space became larger than the particle diameter. SiO_2 particles could easily move out from the sand space. So the normal stress corresponding to the same shear rate increased with increasing of the mesh numbers. When the mesh number was larger than 6000, the sand diameter and sand space became smaller than the particle diameter. SiO_2 particles were above the sand space rather than entering it. The resistance of particle movements would be reduced and then the normal stress corresponding to the same shear rate decreased with the increasing mesh numbers. The combined effect of squeeze velocity and wall roughness on the squeeze flow behavior of STF was shown in figure 8. At each squeeze velocity, peak normal stress was achieved when the mesh

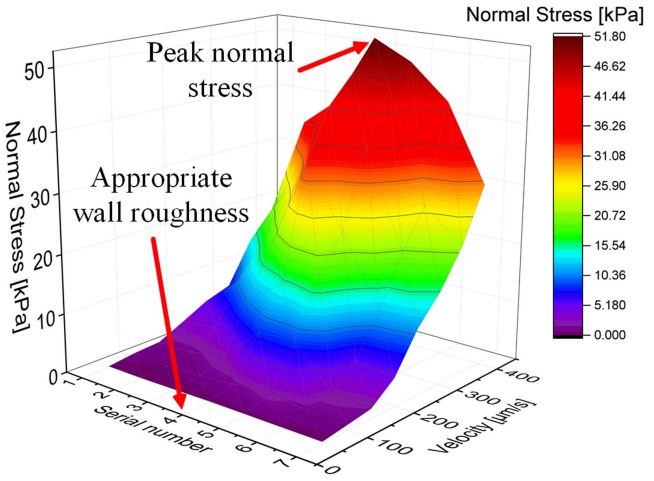

Figure 8. Combined effect of squeeze velocity and wall roughness on the normal stress.

number of plastic sandpaper was 6000. Roughness would strengthen the interactions between sample and wall. When the sand space and sand diameter were similar to the size of SiO_2 particles, normal stress of STF under squeeze conditions was enhanced to the greatest extent. When choosing the appropriate wall roughness, the peak normal stress could reach 51.76 kPa. Compared with the quartz crystal wall, the peak normal stress increased by 34.5%.

3.5. Effect of squeeze on the shear viscosity

Shear viscosity of STF was closely associated with the inner structure evolution [25]. Squeeze apparently affected the distributions of SiO_2 particles in STF. Thus, squeeze showed obvious effect on the shear viscosity. In the squeeze-tensile test, a constant shear rate was applied on STF. Mass fraction of the sample was 71 wt%. Under the combined effects of shear and squeeze, the shear viscosity of STF was closely related to the gap (figure 9(a)). In figure 9(b), the variation of shear viscosity could be divided into three stages: steady shear, squeeze and tensile. In the steady shear stage, the shear rate was 25 s^{-1} and the gap was kept at 1 mm. Shear viscosity was very small at this stage, which meant that STF did not reach the shear thickening state. In the squeeze stage, the shear rate and squeeze velocity were set as 25 s^{-1} and 50 $\mu m\,s^{-1}$, respectively. Shear viscosity increased slightly at first. After the gap decreased to a critical value, a rapid viscosity growth could be seen. In the tensile stage, shear viscosity apparently decreased with the increasing gap. It is important to notice that shear viscosity almost changed simultaneously with the normal stress.

In order to investigate the influence of squeeze velocity on shear viscosity, shear rate was fixed at 10 s^{-1} while squeeze velocity varied from 50 to 500 $\mu m\,s^{-1}$. At the same gap, shear viscosity increased with increasing of the squeeze velocity (figure 9(c)). Meanwhile, the critical gap for shear thickening also increased. Contacts and frictions between particles played an important role in the rheological property of STF [3–5]. In the absence of squeeze, it is found that the test gap had a significant effect on shear viscosity. Under squeeze, both test gap and squeeze velocity could determine the shear viscosity [30]. SiO_2 particles in STF were spread out radially between the parallel plates in the squeeze procedure. When the squeeze velocity was 50 $\mu m\,s^{-1}$, the diffusion of particles was smooth. So there was only a slight increment in shear viscosity at this squeeze velocity. With increasing of the squeeze velocity, the diffusion of particles was impeded. Particles began to contact with each other and formed particle chains. Accompanied by the increment of normal stress, friction between particles became more obvious, resulted in the increment of shear viscosity [34]. In the tensile condition, gap grew large and normal stress was released. Distance between particles became large. So shear viscosity decreased in this condition.

In the squeeze procedure, shear rate also had a great effect on the shear viscosity. In figure 9(d), squeeze velocity was fixed at 50 $\mu m\,s^{-1}$ while shear rate was varied from 10 to 30 s^{-1}. As discussed above, there was only a slight increment in shear viscosity when shear rate was 10 s^{-1}. As shear rate changed from 10 to 30 s^{-1}, shear viscosity grew from 0.53 to 33.34 Pa s and the critical gap obviously increased. When the shear rate was 10 s^{-1}, the measured sample was at the state of shear thinning. Particles were almost uniformly distributed and no cluster was formed in the sample. The slight increment in viscosity was due to the decrement of the gap. With increasing of the shear rate, particles moved close to each other and small-scale clusters were formed. As the sample continued to be squeezed, the distance between particles reduced. The small-scale clusters contacted with each other and formed particle chains. At this time, both normal stress and interparticle friction increased, resulted in the increment of shear viscosity. The measured sample changed into the shear thickening state. By applying squeeze or tensile conditions on sheared STF, we found that shear viscosity was easily affected by the shear rate and squeeze velocity. Together with shear, squeeze could change the inner particle distributions and caused the changes of shear viscosity in STF. It could be concluded that moving boundary had significant influences on the rheological property of STF. With these results, designing an STF-based damper under a combining mode of squeeze and shear would obviously promote its working efficiency.

4. Conclusion

In this work, the squeeze flow behavior of STF was investigated under constant volume. In the squeeze procedure, there was an obvious increase in normal stress due to formation of particle chains and alignment of clusters. STF under squeeze mode could provide larger peak stress (38.48 kPa) than shear mode (6.38 kPa). Thus, developing new STF devices under squeeze flow mode could significantly improve the working efficiency. The influences of squeeze velocity and mass fractions on the squeeze flow behavior of STF were systematically studied. With increasing of the squeeze velocity and mass fraction, both the normal stress and critical gap of STF

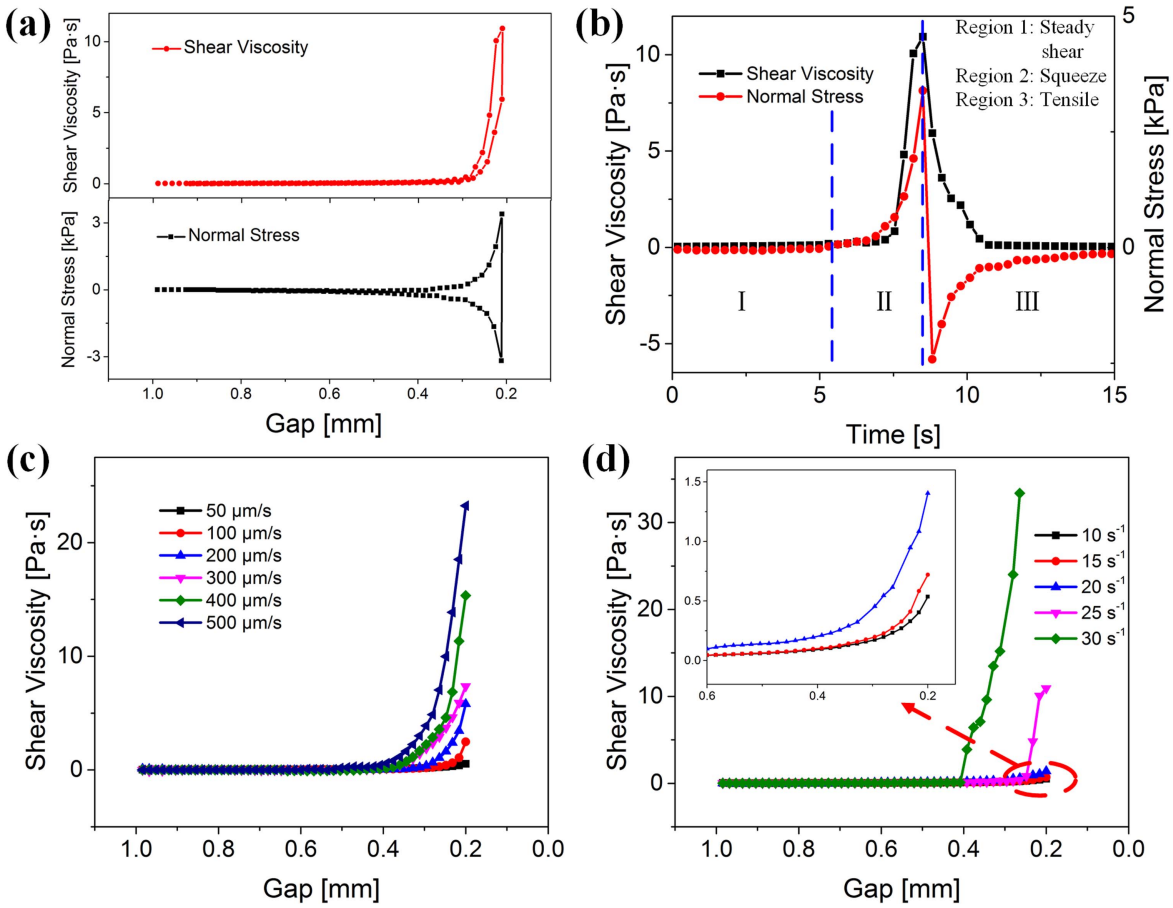

Figure 9. (a) and (b) The variation of shear viscosity and normal stress during one squeeze-tensile cycle; (c) effect of squeeze velocity on shear viscosity; (d) effect of shear rate on shear viscosity. Mass fraction of the sample was 71 wt%.

significantly increased. Plastic sandpaper was used to change the wall roughness in the squeeze experiment. When the size of plastic sands was similar to the SiO_2 particles, the normal stress of STF was greatly increased. Moreover, a constant shear was conducted on the squeezed STF to investigate the variation of shear viscosity under the squeeze mode. Under moving boundary, there was an obvious increment in shear viscosity with the increasing squeeze velocity. Squeeze would accelerate the formation of particle chains and bring forward shear thickening phenomenon. The related squeeze flow behavior of STF was helpful for further understanding the shear thickening mechanism and developing new STF-based devices.

Acknowledgments

Financial supports from the National Natural Science Foundation of China (Grant No. 11372301), the Strategic Priority Research Program of the Chinese Academy of Sciences (Grant No. XDB22040502) and the Fundamental Research Funds for the Central Universities (WK2480000002) are gratefully acknowledged. This work is supported by Collaborative Innovation Center of Suzhou Nano Science and Technology.

References

[1] Barnes H A 1989 Shear-thickening (dilatancy) in suspensions of nonaggregating solid particles dispersed in Newtonian liquids *J. Rheol.* **33** 329–66
[2] Fall A, Bertrand F, Ovarlez G and Bonn D 2012 Shear thickening of cornstarch suspensions *J. Rheol.* **56** 575–91
[3] Peters I R, Majumdar S and Jaeger H M 2016 Direct observation of dynamic shear jamming in dense suspensions *Nature* **532** 214–7
[4] Wagner N J and Brady J F 2009 Shear thickening in colloidal dispersions *Phys. Today* **62** 27–32
[5] Wyart M and Cates M E 2014 Discontinuous shear thickening without inertia in dense non-Brownian suspensions *Phys. Rev. Lett.* **112** 098302
[6] Brown E and Jaeger H M 2014 Shear thickening in concentrated suspensions: phenomenology, mechanisms and relations to jamming *Rep. Prog. Phys.* **77** 046602
[7] Fernandez N, Mani R, Rinaldi D, Kadau D, Mosquet M, Lombois-Burger H, Cayer-Barrioz J, Herrmann H J, Spencer N D and Isa L 2013 Microscopic mechanism for shear thickening of non-Brownian suspensions *Phys. Rev. Lett.* **111** 108301
[8] Gurgen S, Li W H and Kushan M C 2016 The rheology of shear thickening fluids with various ceramic particle additives *Mater. Des.* **104** 312–9
[9] Tan Z H, Zuo L, Li W H, Liu L S and Zhai P C 2016 Dynamic response of symmetrical and asymmetrical sandwich plates with shear thickening fluid core subjected to penetration loading *Mater. Des.* **94** 105–10

[10] Zhou H, Yan L X, Jiang W Q, Xuan S H and Gong X L 2016 Shear thickening fluid-based energy-free damper: design and dynamic characteristics *J. Intell. Mater. Syst. Struct.* **27** 208–20
[11] Smith M I, Besseling R, Cates M E and Bertola V 2010 Dilatancy in the flow and fracture of stretched colloidal suspensions *Nat. Commun.* **1** 114
[12] Wang D H and Liao W H 2011 Magnetorheological fluid dampers: a review of parametric modelling *Smart Mater. Struct.* **20** 023001
[13] Zhu X C, Jing X J and Cheng L 2012 Magnetorheological fluid dampers: a review on structure design and analysis *J. Intell. Mater. Syst. Struct.* **23** 839–73
[14] de Vicente J, Klingenberg D J and Hidalgo-Alvarez R 2011 Magnetorheological fluids: a review *Soft Matter* **7** 3701–10
[15] Wang H Y, Bi C, Kan J W, Gao C F and Xiao W 2011 The mechanical property of magnetorheological fluid under compression, elongation, and shearing *J. Intell. Mater. Syst. Struct.* **22** 811–6
[16] Guo C Y, Gong X L, Xuan S H, Yan Q F and Ruan X H 2013 Squeeze behavior of magnetorheological fluids under constant volume and uniform magnetic field *Smart Mater. Struct.* **22** 045020
[17] Xu Y G, Gong X L, Liu T X and Xuan S H 2014 Squeeze flow behaviors of magnetorheological plastomers under constant volume *J. Rheol.* **58** 659–79
[18] McIntyre E C and Filisko F E 2007 Squeeze flow of electrorheological fluids under constant volume *J. Intell. Mater. Syst. Struct.* **18** 1217–20
[19] Sherwood J D and Durban D 1996 Squeeze flow of a power-law viscoplastic solid *J. Non-Newtonian Fluid Mech.* **62** 35–54
[20] Lian G P, Xu Y, Huang W B and Adams M J 2001 On the squeeze flow of a power-law fluid between rigid spheres *J. Non-Newtonian Fluid Mech.* **100** 151–64
[21] Huang W B, Xu Y, Lian G P and Li H Y 2002 Squeeze flow of a power-law fluid between two, rigid spheres with wall slip *Appl. Math. Mech.* **23** 811–8
[22] Davidson D A and Sammakia B G 2009 Squeezing flow of a power law fluid between grooved plates *J. Electron. Packag.* **131** 031007
[23] Sherwood J D 2011 Squeeze flow of a power-law fluid between non-parallel plates *J. Non-Newtonian Fluid Mech.* **166** 289–96
[24] Chellamuthu M, Arndt E M and Rothstein J P 2009 Extensional rheology of shear-thickening nanoparticle suspensions *Soft Matter* **5** 2117–24
[25] White E E B, Chellamuthu M and Rothstein J P 2010 Extensional rheology of a shear-thickening cornstarch and water suspension *Rheol. Acta* **49** 119–29
[26] Teng H X and Zhang J J 2013 A new thixotropic model for waxy crude *Rheol. Acta* **52** 903–11
[27] Chen Q, Xuan S H, Jiang W Q, Cao S S and Gong X L 2016 Shear time dependent viscosity of polystyrene-ethylacrylate based shear thickening fluid *Smart Mater. Struct.* **25** 045005
[28] Mukherjee A, Sharma D, Chauhan S S and Singh H 2015 Time-dependent and shear-dependent transient viscosity of an alumina suspension *J. Dispersion Sci. Technol.* **36** 951–69
[29] Hegger C and Maas J 2016 Investigation of the squeeze strengthening effect in shear mode *J. Intell. Mater. Syst. Struct.* **27** 1895–907
[30] Fall A, Huang N, Bertrand F, Ovarlez G and Bonn D 2008 Shear thickening of cornstarch suspensions as a reentrant jamming transition *Phys. Rev. Lett.* **100** 018301
[31] Ye F, Zhu W, Jiang W Q, Wang Z Y, Chen Q, Gong X L and Xuan S H 2013 Influence of surfactants on shear-thickening behavior in concentrated polymer dispersions *J. Nanopart. Res.* **15** 2122
[32] Wang S, Xuan S H, Jiang W Q, Jiang W F, Yan L X, Mao Y, Liu M and Gong X L 2015 Rate-dependent and self-healing conductive shear stiffening nanocomposite: a novel safe-guarding material with force sensitivity *J. Mater. Chem.* A **3** 19790–9
[33] Zhao X P and Gao D J 2001 Structure evolution in Poiseuille flow of electrorheological fluids *J. Phys. D: Appl. Phys.* **34** 2926–31
[34] Mari R, Seto R, Morris J F and Denn M M 2014 Shear thickening, frictionless and frictional rheologies in non-Brownian suspensions *J. Rheol.* **58** 1693–724